Supporting Information

Zhou et al. 10.1073/pnas.1500953112

SI Materials and Methods

Data Analysis. Single-channel data were analyzed with the threshold-based single-channel search function of Clampfit 9.2 (Molecular Devices). The conductance–potential (G–V) relationship of BK currents was constructed from isochronal tail current measured at 100 μs after variable test steps. The G–V curve was fit with the Boltzmann function to determine the potential for half-maximal activation (V_h) and apparent equivalent gating charge (z):

$$G(V) = \frac{G_{\max}}{1 + \exp\left(\frac{zF(V_h - V)}{RT}\right)},$$

where F, R, and T have their usual physical meanings. The inhibition dose–response curves in Fig. 3 *D1–D5* were fit with a Hill equation

$$\frac{I_{Cd}}{I_{ctrl}} = \frac{1}{1 + \left(\frac{[Cd^{2+}]}{IC_{50}}\right)^n},$$

where n is Hill coefficient and IC_{50} is $[Cd^{2+}]$ blocking 50% of BK current. Statistical analysis and curve fitting were performed with OriginPro 7.5 (OriginLab Corporation). Mean values are presented as mean ± SEM.

Molecular Modeling. Radius profiles of Kv1.2 and KcsA channels shown in Fig. 1*B* are calculated from their crystal structures using program HOLE (1). The homology model of the BK PGD shown in Fig. 5 was generated in Modeler (2) by using the Kv1.2 structure (PDB ID code 2A79) as a template. Structural adjustment and energy minimization were performed in UCSF Chimera (3), with default parameters used for energy minimization. In Fig. 5, valines of BK_{319} and $Kv1.2_{406}$ are replaced by cysteines, and valine of $Kv1.2_{408}$ is replaced by glutamate using the swapaa function in UCSF Chimera. The structure images in Fig. 5 were prepared using UCSF Chimera.

1. Smart OS, Neduvelil JG, Wang X, Wallace BA, Sansom MS (1996) HOLE: A program for the analysis of the pore dimensions of ion channel structural models. *J Mol Graph* 14(6):354–360, 376.
2. Sali A, Blundell TL (1993) Comparative protein modelling by satisfaction of spatial restraints. *J Mol Biol* 234(3):779–815.
3. Pettersen EF, et al. (2004) UCSF Chimera—a visualization system for exploratory research and analysis. *J Comput Chem* 25(13):1605–1612.

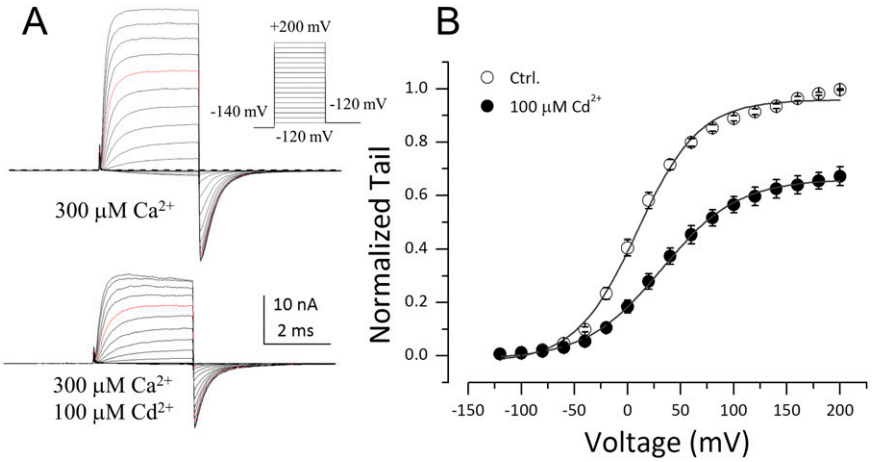

Fig. S1. The leftward-gating shift of Cd^{2+} in the presence of 300 μM Ca^{2+} is partially dependent on the low-affinity divalent cation binding site E399. (*A*) Macroscopic currents of mSlo1E399A recorded in the absence (*Upper*) and presence (*Lower*) of 100 μM intracellular Cd^{2+}. (*B*) G–V relationships of E399A in 300 μM Ca^{2+} in the absence (open symbols) or presence (filled symbols) of 100 μM Cd^{2+}. Boltzmann fit results (line) are z = 0.9e, V_h = +9 mV (control); z = 0.7e, V_h = +37 mV (100 μM Cd^{2+}).

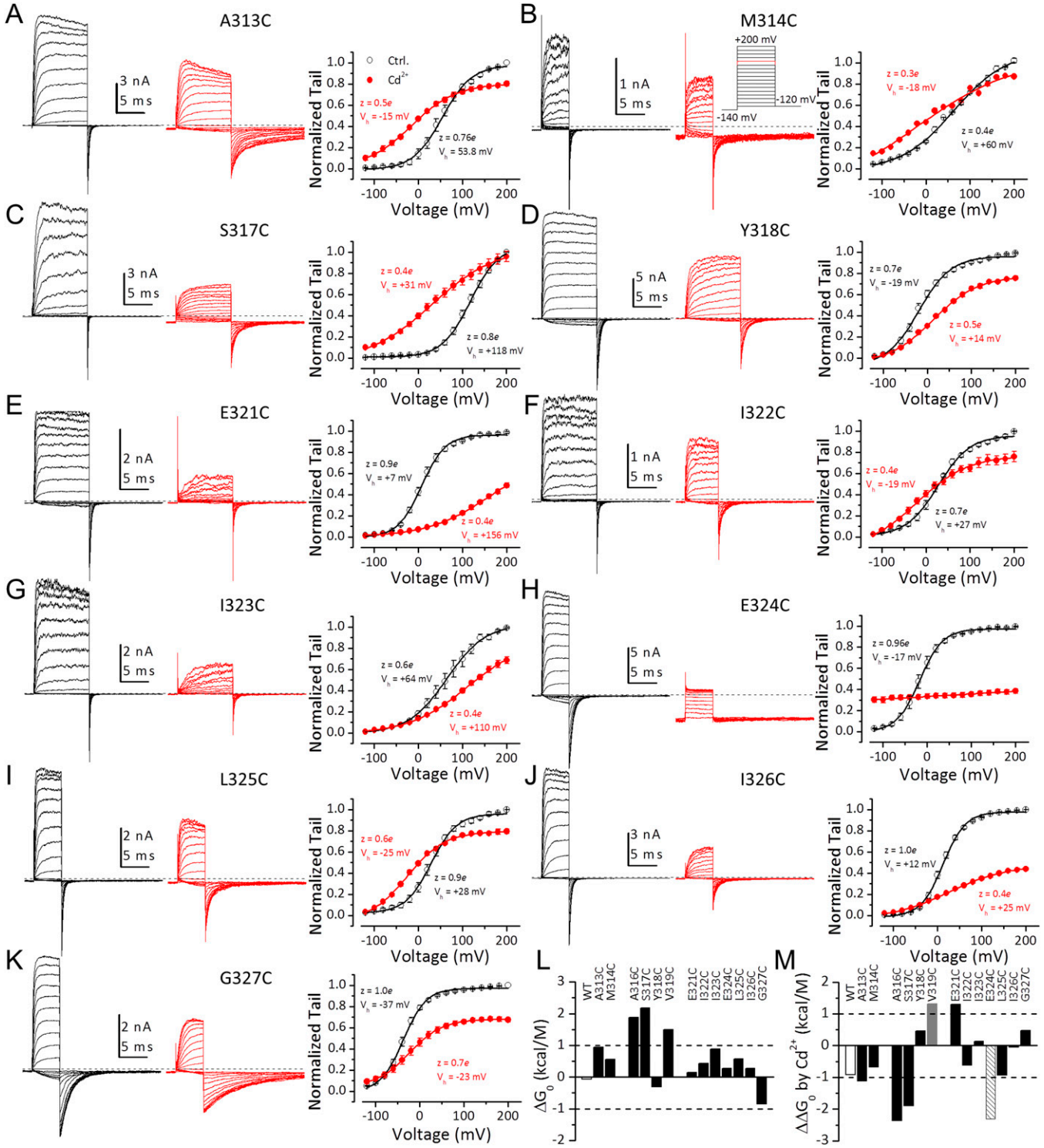

Fig. S2. Basic gating properties of BK S6 cysteine mutants. (*A–K*) Currents of BK S6 cysteine mutants recorded in 300 μM Ca^{2+} without (black) or with (red) 100 μM Cd^{2+}. Zero current level is indicated by dotted line. *G–V* plots are on the right of each pair of sample traces, with Boltzmann fit results (lines) included (black: ctrl; red: Cd^{2+}). (*L*) Gibbs free energy between closed and open states at 0 mV (ΔG_0) of wild-type (open) and S6 cysteine mutants (filled) in 300 μM Ca^{2+}. $\Delta G_0 = 0.2389zFV_h$, in which F is the Faraday's constant. Apparent equivalent gating charge z and half-maximal activation potential V_h are determined from Boltzmann fit of average *G–V*. (*M*) Change of ΔG_0 ($\Delta\Delta G_0$) of the wild-type (open) and S6 cysteine mutants (filled) in 100 mM Cd^{2+}. $\Delta\Delta G_0 = \Delta G_{0\ Cd} - \Delta G_{0\ Ctrl}$. The z and V_h of V319C (gray) in Cd^{2+} was determined from Boltzmann fit of *G–V* simulated with the Horrigan–Aldrich model, assuming VSD–PGD coupling factor D decreases from 25 to 6 in 100 μM Cd^{2+}. The V_h of E324C (stripe) in 100 μM Cd^{2+} is more negative than −200 mV (*H*), and the minimal $\Delta\Delta G_0$ of E324C was estimated by using V_h of −200 mV and z of 0.44 (mean value of z of all other 12 S6 cysteine mutations in 100 μM Cd^{2+}) in 100 μM Cd^{2+}.

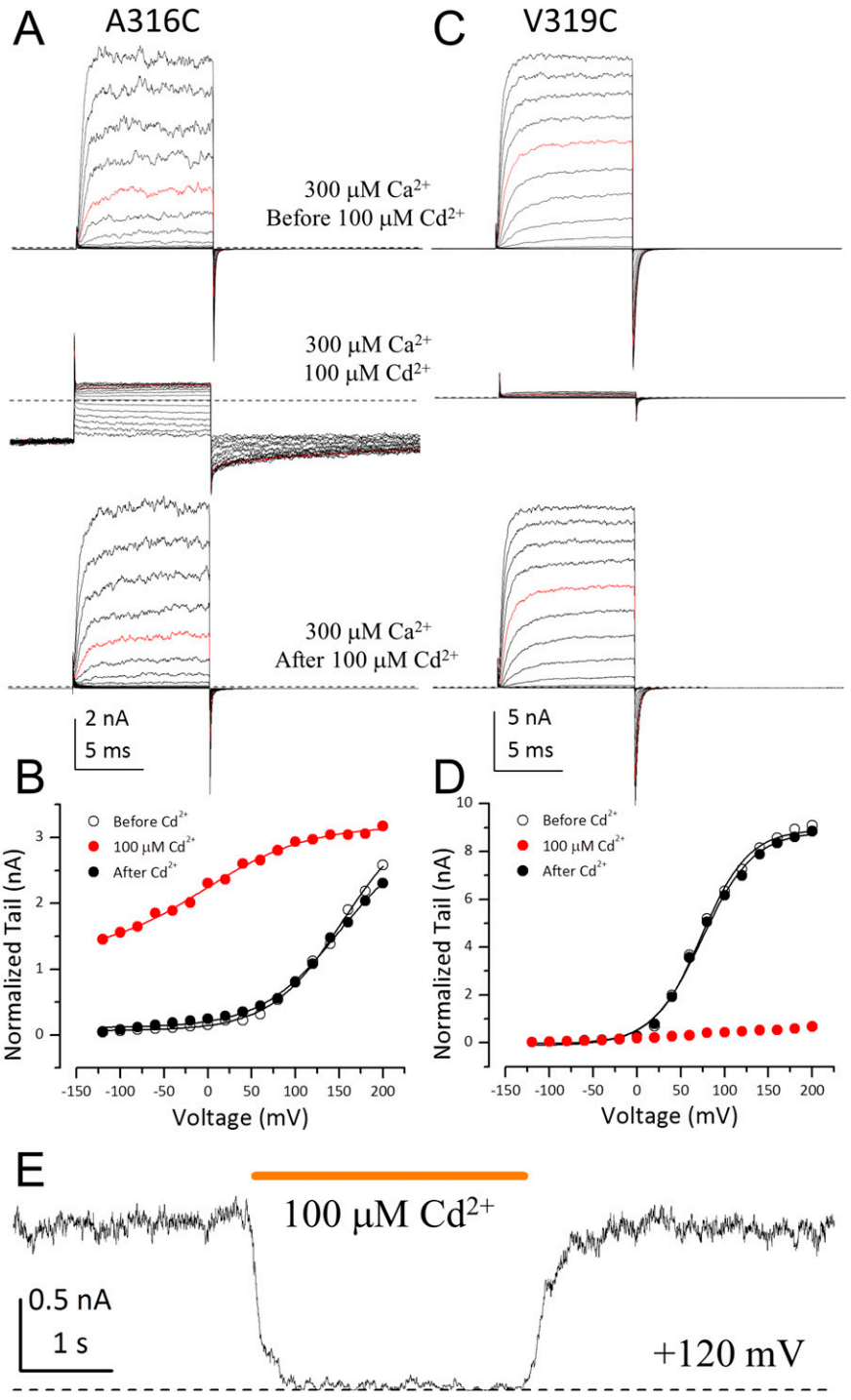

Fig. S3. Cd^{2+} coordination with A316C or V319C is reversible. (*A*) Macroscopic currents of A316C recorded in 300 μM Ca^{2+} before (*Top*), during (*Middle*), and after (*Bottom*) perfusion in 100 μM Cd^{2+}. (*B*) *G–V* relationships of A316C in 300 μM Ca^{2+} before (open), during (red filled) and after (black filled) perfusion in 100 μM Cd^{2+}. Boltzmann fit results (line) are $z = 0.6e$, $V_h = +153$ mV (before); $z = 0.42e$, $V_h = -4$ mV (during); $z = 0.6e$, $V_h = +149$ mV (after). (*C*) Macroscopic currents of V319C recorded in 300 μM Ca^{2+} before (*Top*), during (*Middle*), and after (*Bottom*) perfusion in 100 μM Cd^{2+}. (*D*) *G–V* relationships of A316C in 300 μM Ca^{2+} before (open), during (red filled), and after (black filled) perfusion in 100 μM Cd^{2+}. Boltzmann fit results (line) are $z = 0.9e$, $V_h = +73$ mV (before); $z = 0.9e$, $V_h = +74$ mV (after). (*E*) V319C current recorded at +120 mV in 300 μM Ca^{2+}. Application of 100 μM Cd^{2+} is indicated by orange bar. Zero-current level is indicated by dotted line.

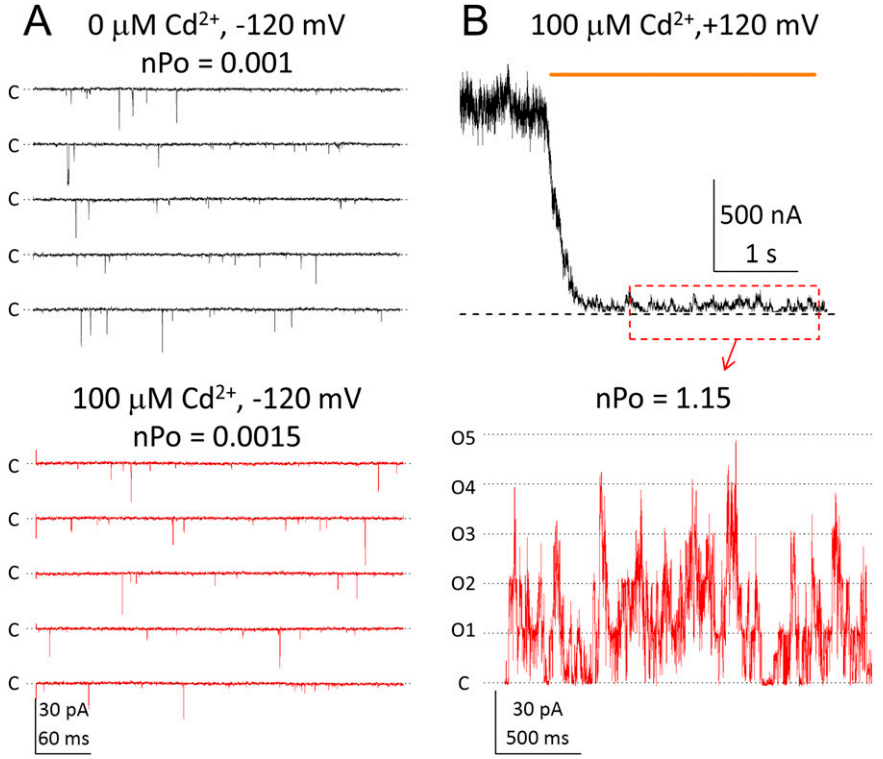

Fig. S4. Cd^{2+}-V319C coordination does not inhibit BK channel activity at negative potentials. (*A*) Single-channel activity of V319C recorded at –120 mV with 300 μM Ca^{2+} in the absence (*Upper*) and presence (*Lower*) of 100 μM intracellular Cd^{2+}. The nPos in control solution and Cd^{2+} solution were 0.001 and 0.0015, respectively. Base lines are indicated by dotted lines. The ratio of nPo_{Cd}/nPo_{Ctrl} is 1.36 ± 0.2 (n = 5) at –120 mV, and the ratio of I_{Cd}/I_{Ctrl} is 0.09 ± 0.02 (n = 6) at +120 mV (Fig. 2*D*). nPo was determined from steady-state recordings of 10- to 30-s duration. (*B*) V319C current recorded at +120 mV from the same patch shown in *A* before and during perfusion of 100 μM Cd^{2+}. The nPo of the segment recorded in 100 μM Cd^{2+} (*Lower*) is 1.15.

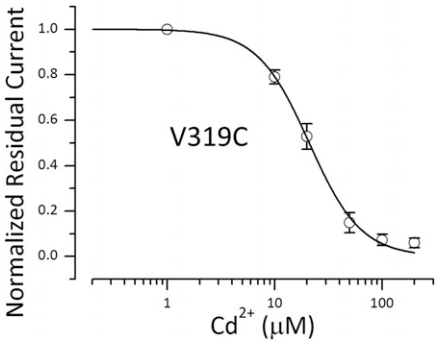

Fig. S5. Concentration–response curve of Cd^{2+}-V319C coordination determined at 0 mV in the presence of 300 μM Ca^{2+}. Residual current was examined by 2-ms test pulses to +160 mV every second. Line corresponds to fit of an inhibitory Hill equation with IC_{50} = 21 μM and n = 1.8.

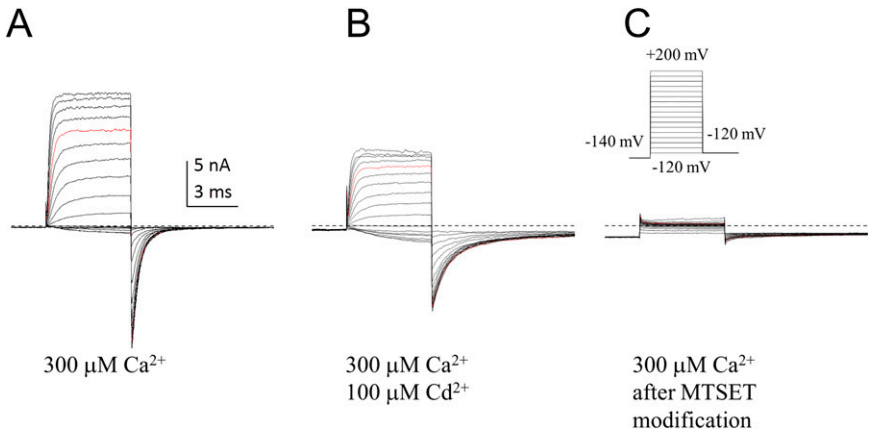

Fig. S6. V319C can still be modified by intracellular MTSET in the V319CE321Q construct. (*A*) Macroscopic V319CE321Q currents recorded in control solution. (*B*) Currents recorded from the same patch in *A* in the presence of 100 μM Cd^{2+}. (*C*) Currents recorded in control solution after perfusion in 1 mM MTSET at +60 mV for 15 s. Modification of V319C is indicated by the strong inhibition of outward current after perfusion in MTSET.

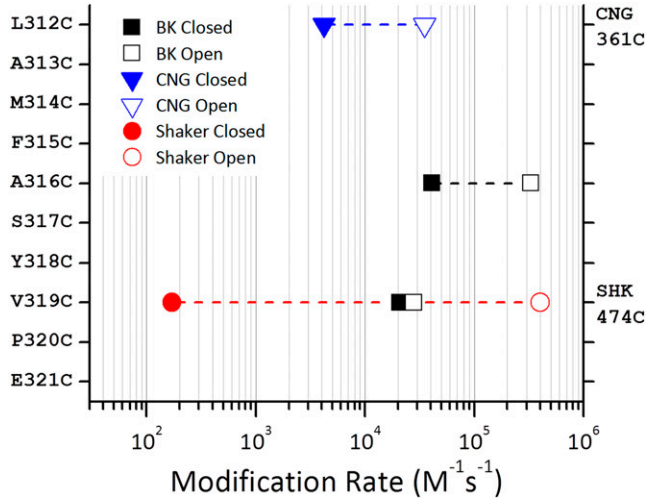

Fig. S7. Second-order rate constants of Cd^{2+} coordination with BK V319C or A316C in closed (filled square) and open (open square) states plotted on logarithmic scale. Results from CNG (1) (triangle) and Shaker channels (2) (circle) are plotted for comparison.

1. Contreras JE, Srikumar D, Holmgren M (2008) Gating at the selectivity filter in cyclic nucleotide-gated channels. *Proc Natl Acad Sci USA* 105(9):3310–3314.
2. del Camino D, Yellen G (2001) Tight steric closure at the intracellular activation gate of a voltage-gated K(+) channel. *Neuron* 32(4):649–656.

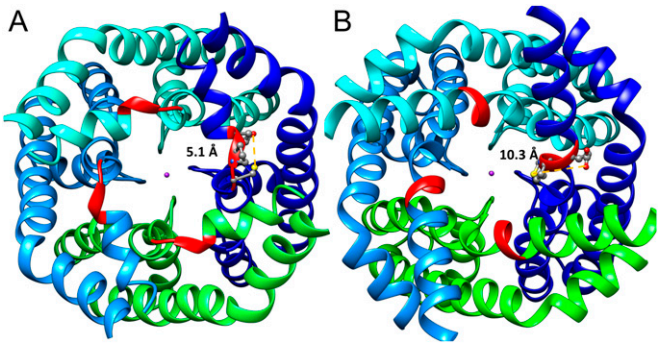

Fig. S8. Cartoon of a theoretical BK PGD based considerations given in the text (*A*) and the Kv PGD from the Kv1.2 crystal structure (PDB ID code 2A79) (*B*) viewed from their cytosolic entrances. Each subunit is rendered in distinct colors. The CPE triplets are colored in red. The side chains of the triplet in one subunit are rendered as ball and chain with distances between Glu(Oδ) and Cys(S) marked by orange dotted lines. The purple dots in the center are potassium ions.